Fabrication of nanophotonic devices for single-photon applications.

Charlie Ellcome

School of physics and astronomy, University Of Southampton, Southampton , UK

April 30, 2019

Abstract

The surface between a metal and a non-metal surface can support oscillations in charge densities. These plasmons can be used to improve the emission of a photon source into free space. This effect can be applied to diamond nitrogen valency centres in order to increase the rate of collectable single photon emission. Computational simulations imply that the degree of enhancement obtained depends on the architecture of these plasmonic devices. Computerised simulations of maltese cross shapes suggest a maximum enhancement of 1.7. Manufactured maltese crosses produce an enhancement of 1.57 ± 0.51. Which shows promise in the utilization of such devices to increase the collectable emissions of diamond nitrogen valency centres.

1 Introduction

1.1 Single Photon Sources

Single Photon Sources have a number of potential uses. The field where they possess the greatest interest is the field of quantum communications. While a number of theoretical quantum communications protocols boast not only unbreakable encryption but also the potential to detect the presence of any intercepting parties (Kuppam, 2018) in practice this is only true if the communication is mediated through single photons. Pulses of light allow eavesdropping parties to effectively skim information without having to interact with the entire pulse not only making them much more difficult to detect but more likely to intercept a part of the message being sent. While methods of detecting eavesdroppers on such pulsed light systems do exist they are less than ideal. Requiring conditions which have to be arranged ahead of time (invalidating one of the advantages of quantum communications) and result in slowing down of the communication process. This and due to the probabilistic nature of quantum communications they are not perfect systems for detecting such eavesdroppers. (Shrivastava and Verma, 2012)

1.2 Negatively charged nitrogen valency centres as single photon sources

A number of sources of single photon emission exist. Colour centres or synonymously defects in crystal structure are an example of these. Each having several properties which affects the way in which they can be used. Diamond crystal structure results in a number of physical properties, such as its high thermal conductivity and hardness, which make single photon sources based in diamond more stable than those based on other materials. (Aharonovich, Greentree and Prawer, 2011) This stability being particularly attractive as such single photon sources will not need to be replaced as often as other but also allows diamond based single photon sources to be used under a greater range of conditions. Nitrogen Valency centres of diamond have further attractive properties when compared to other colour centres of diamond. First is that diamond nitrogen valency centres can be pumped in the visible regime of light and will also emit in the visible regime of light. This meaning that technologies relying on single photon sources would not require more expensive optical equipment capable of operating outside the visible light range. Second is that, when compared to other diamond colour centres, the diamond nitrogen valency centres are probabilistically the most likely to form. Making manufacture easier resulting in them being more common and thereby cheaper than other diamond colour centre alternatives. (Alkahtani et al., 2018).

Unfortunately the disadvantage diamond nitrogen valency centres have as a source of single photons is their comparatively low emission rates. Quantum dot single photon sources have emission rates starting at 500 megahertz while diamond nitrogen valency centres have maximum emission rates of 360 megahertz. (Santori, Fattal and Yamamoto, 2010) As such to be a competitive source of single photons the extractable emission from diamond nitrogen valency centres would have to be optimised.

2 Enhancement of emission

2.1 The Purcell effect

The Purcell effect is the method of increasing the emission rate of a photon source utilising and optical cavity and has been used to increase the emission rate of other single photon sources. (Reithmaier et al., 2004) Unfortunately this method is not compatible with diamond nitrogen valency centres. Diamond colour centres, including diamond nitrogen valency centres, being a defect in the lattice structure of diamond which results in a variation in the electron distribution in the lattice and this is how the single photon source is formed. The optical properties of the colour centre being how this discontinuity compares to the surrounding environment. As such diamond colour centres are sensitive to their surroundings. As the enhancement in the rate of emission due to the Purcell effect is inversely proportional to the modal volume of the optical cavity as proven by:

$$Enhancement = \frac{3}{4\pi^2}(\frac{\lambda_{free}}{n})^3(\frac{Q}{V_m})$$

So to gain a greater emission rate the optical cavity is small enough to result in the changing of the diamond colour centre's surroundings. Changing the absorption and emission properties of diamond nitrogen valency centre can not only invalidate the advantage that it absorbs and emits in the visible regime of light but also has the potential to detune the diamond nitrogen valency centre from the constructed optical cavity. This making the coupling between diamond nitrogen valency centres and optical cavities more difficult than other single photon sources. (Santori, Fattal and Yamamoto, 2010)

2.2 Optical techniques

It being difficult to increase the rate with which diamond nitrogen valency centres emit at an alternative is to maximise the amount of emission that can be used. Diamond has a refractive index of 2.41 (Phillip and Taft, 1964). This results in a critical angle of 24.5 degrees when transmitting directly into free space which, if coupling light from a flat diamond surface in a given direction will represent less than 5% of the emission of the diamond nitrogen valency centre actually making it to where it can be used. While a sphere of diamond can be used to mitigate the critical angle (as light from the centre of the sphere will always be normal to the surface) in practice not only is it exceptionally difficult to make a sphere of diamond, due to diamond's physical properties which make it so attractive as a single photon source in the first place, but also due to the probabilistic nature of producing diamond nitrogen valency centres there is no guarantee that emission will be coming from the centre of the sphere. As such nanoscopic diamond is used. While the results may not be as ideal as a perfect sphere of diamond with a nitrogen valency centre in the middle due to its size the radius of curvature can

drastically reduce the effect of the critical angle. Moreover nanodiamonds with nitrogen valency centres are easier to manufacturer than bulk diamond with useable nitrogen valency centres. However taking this into consideration, with it being impossible to utilise lone diamonds on the nanoscale, the act of imbedding such nanodiamonds into a material with a lower refractive index can increase the critical angle and hence increase the proportion of collectable emissions.

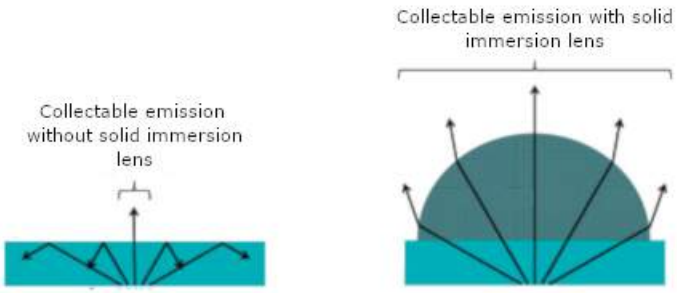

Figure 1: *A ray diargram showing the use of a solid immersion lens in order to increase the collectable emissions from a point like source. Left: Emission without solid immersion lens. Right: Emission with the use of a solid immersion lens.*

The use of solid immersion lenses can be used to further optimise the collectable emissions from this solid state system as demonstrated in figure 1. There is however a limit as to how well such techniques can improve the collectable emission from the diamond nitrogen valency centre. This diffraction limit imparts a limit depending on the wavelength of light and the refractive index of where the emission is being directed. The wavelength of light being defined by the diamond nitrogen calency centre cannot be changed. While the refractive index where emission is being directed can potentially be changed this is not ideal as it would either require complicated equipment which mitigates the advantage that diamond single photon sources can be used in a range of environments.

2.3 Plasmonic techniques

Light incident on a surface between a metal and a non-metal can generate oscillations in charge densities. These surface plasmons can in turn be manipulated by how the surface between the metal and non-metal changes. When utilised on a nanoscopic scale plasmons can result in changing the collectable emissions from a light source in two ways. Plasmons can either resonate with photons in order to produce enhancement not dissimilar to a feedback loop, or plasmons interact with photons causing the photons to scatter. Which one of these occurs and weather these results in an enhancement or reduction of emission depends on both the shape of the interface and how the size of the interface corresponds with the wavelength of light from the photon source. Such nanophotonic devices have been studied before, with a multitude of different shapes, scales and enhancing wavelengths. Theory suggests that many different shapes ranging

from solid disks to pairs of triangles can result in the enhancement of light. (Hao and Schatz, 2004) Each having their own degree of enhancement and limitations as to the light they can enhance. In depth study of these dual triangle, bowtie, shapes reveals that while enhancement can occur in the infra-red regime and cover a range of wavelengths spanning hundreds of nanometres the dimensions of these devices effects not only the degree of enhancement, but the wavelength that receives the optimum enhancement (Kino et al., 2007). Other studies have revealed ring shapes also enhance light, although with a lesser magnitude, at visible wavelengths. (Trojak et al., 2017)

2.4 Optimisation of enhancement

As the enhancement due to plasmonic manipulation techniques is not limited by the diffraction limit of more traditional optical techniques not only can use of such plasmonic techniques potentially increase the collectable emissions from diamond nitrogen valency centres but can also potentially be used alongside more traditional optical techniques in order to fully optimise the collectable emissions utilising these two effects.

3 Computational simulations of plasmonic enhancement

As there is a wide range of potential architectures for plasmonic devices, each with their own properties, before attempting to create any such devices it is beneficial to first perform computerised simulations of the various architectures in order to determine which nanophotonic devices would result in the greatest enhancement for the emission of diamond nitrogen valency centres and the dimensions of the device in order to do so.

The enhancement due to such plasmonic devices is determined through the use of finite-difference time-domain simulations which solves Maxwell's time dependent curl equations organised in such a way that the electric field is used to determine the Magnetic field strength of adjacent points and the Magnetic field strength used to determine the electric field at all adjacent points (Taflove, 1995). Such simulations have to be carefully defined in order to give accurate results, especially considering the practical limitations of the manufacturing process however once fully defined can not only determine the electric field at any point (and hence the effect of the presence of the plasmonic device) but also can be used to iterate through varying shapes and dimensions in order to determine what architectures and dimensions result in the optimum enhancement and how that optimum enhancement is obtained.

Figure 2 shows the initial condition of the simulated system. A dipole source emulating the emission of the diamond nitrogen valency centre is placed on the surface of the silicon nitride. The layer of Indium Tin Oxide on top of the dipole source representing the need for a material to hold the nanodiamonds in place. The exact effect of this capping layer on the enhancement effects of the plasmonic devices can aslo be determined by such simulations

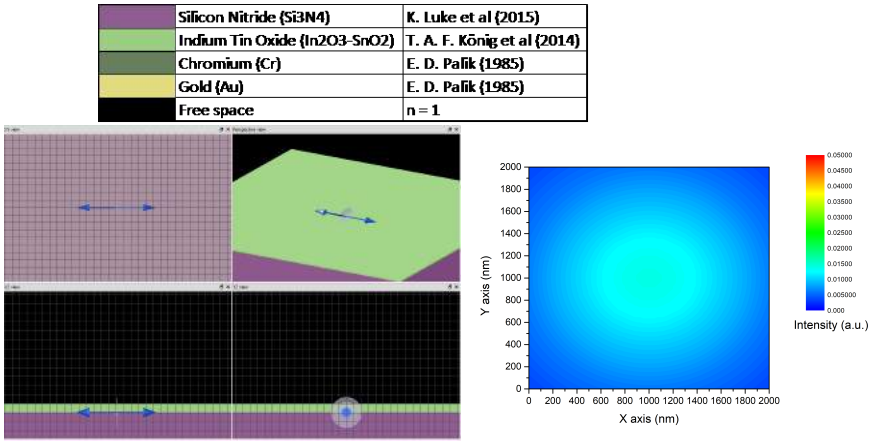

Figure 2: *The initial state of a simultation where a dipole source is used to represent a diamond nitrogen valency centre. Top: The material properites of the simulation region. Left: The simulation region configuration. Right: Output intensity from the simulation region.*

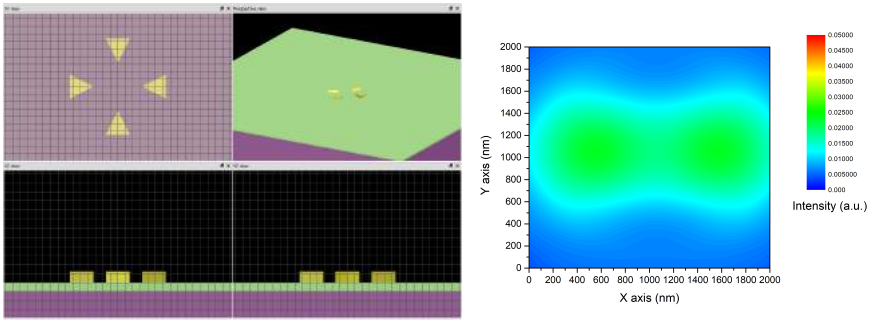

Figure 3: *A simulation of maltese cross shaped plasmonic devices. The left demonstrating the simulation region. The simulations are capable of changing the dimentions of the device in order to maximuise the obtained enhancement. The right representing the maximum output from the simulated system.*

Figure 3 shows a simulation with a maltese cross. Analysis of bowtie shaped plasmonic devices demonstrates that such devices are dependent on polarisation. (Grober, Schoelkopf and Prober, 1997) as such the act of creating two bow tie shapes orientates at 90 degrees from one another can mitigate the fact that diamond nitrogen valency centre emission is unpolarised. However the final result will not be the same as the sum of two bow tie enhancements due to the plasmonic devices coupling to one another. A thin 7nm layer of chromium is included in the simulation as a limitation of the manufacturing process. Being required as an adhesive between the indium tin oxide and gold layers. When the dimensions of the triangles, their thickness and separation, is optimised the emission over the surface increases by a factor of 1.7.

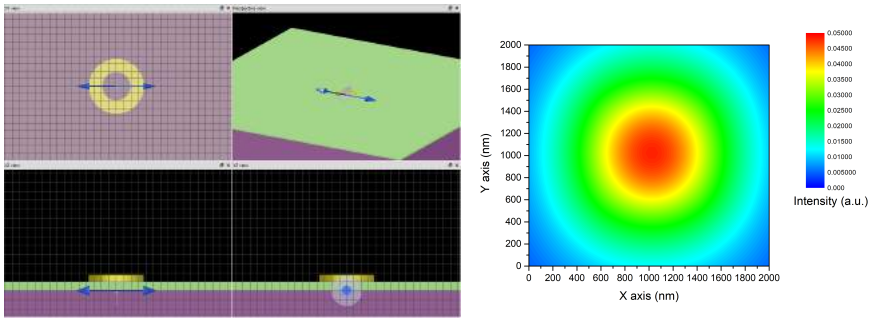

Figure 4: *A simulation of ring shaped plasmonic devices. The left demonstrating the simulation region. The simulations are capable of changing the dimentions of the device in order to maximuise the obtained enhancement. The right representing the output from the simulated system.*

Figure 4 shows a simulation of a single ring. Due to the unpolarised nature of the photon source and the fact that plasmonic rings have already been shown to exhibit an enhancement independent of polarisation in the visible regime of light. (Trojak et al., 2017) When the inner and outer radii alongside the thickness of the ring are optimised the emission is increased by a factor of 3.5.

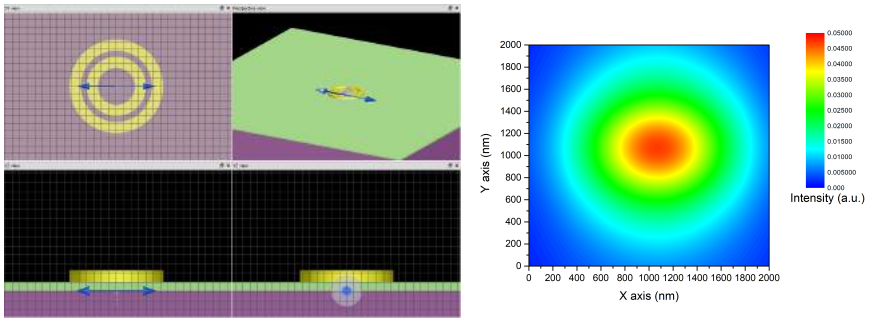

Figure 5: *A simulation of multiple concentric ring shaped plasmonic devices. The left demonstrating the simulation region. The simulations are not only capable of changing the dimentions of the device in order to maximuise the obtained enhancement but also able to change the number of rings. The right representing the maximum output from the simulated system with three rings.*

Figure 5 shows a simulation of multiple concentric rings. All with the same central point but differing radii. Simulation of such concentric rings demonstrated higher enhancements the more rings used however after the addition of the third ring enhancement experiences diminishing returns (the difference between optimised three rings and optimised four rings being an increase of 0.0004). When the dimensions of three concentric rings is optimised an enhancement of 7.2 is theorised. Watching the simulations in action implies that the jump in enhancement between the single and concentric rings is due to the fact that while the maltese cross and single ring

enhancements are due to scattering concentric ring enhancement is due to the plasmonic resonances due to the proximity of the metallic surface between each concentric ring. Plasmonic resonances generating larger enhancement factors than Plasmonic scattering.

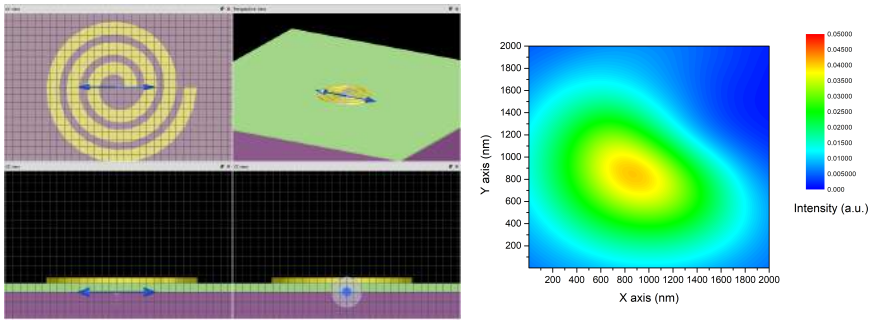

Figure 6: *A simulation of a archimedean spiral shaped plasmonic device. The left demonstrating the simulation region. The simulations are not only capable of changing the dimentions of the device in order to maximuise the obtained enhancement but also able to change the number of times 360 degrees is spanned by the of the spiral. The right representing the maximum output from the simulated system with over 1080 degrees.*

Figure 6 shows a simulation of an archimedean spiral. Watching the simulations in action shows that this too causes an enhancement due to plasmonic resonances which also receives diminishing returns after the addition of the third spiral layer. That said the resulting enhancement of an optimised spiral is a factor of 4.2. Moreover the loss of symmetry from the system redirects power away from being normal to the surface. As the emission from the sample is predicted to emerge and an angle this can result in complication using the emission and so such shapes should be avoided.

4 Practical

4.1 Obtaining diamond nitrogen valency centres for enhancement

As mentioned in section 2.2 bulk diamond is not ideal as a source of diamond nitrogen valency centres. Rather it is more beneficial to use nanoscale diamonds both as a method of increasing enhancement and due to the availability of nanoscale diamonds with nitrogen valency centres within them. The nanodiamonds used are 27nm in scale which due to practicality are stored as a slurry of nanodiamonds and water. However nanodiamonds cannot be used while in this mixture. Mainly due to the fact the nanodiamonds will be constantly moving in the slurry but also due to the fact that when in water nanodiamonds form clumps. The sonification of water alone can reduce nanodiamond clumping size but not eliminate clumping altogether. (Ōsawa, 2008)

The use of small nanodiamond clumps means that these clumps are not single photon sources but rather an ensemble of single photon sources. While not ideal the use of

plasmonic devices can still result in an enhancement of the ensemble. The enhancement will not be uniform, but rather a function as to how close a particular single photon source is to the centre of the plasmonic device. Evidence of this can be obtained from the simulations of plasmonic devices and is shown in figure 7.

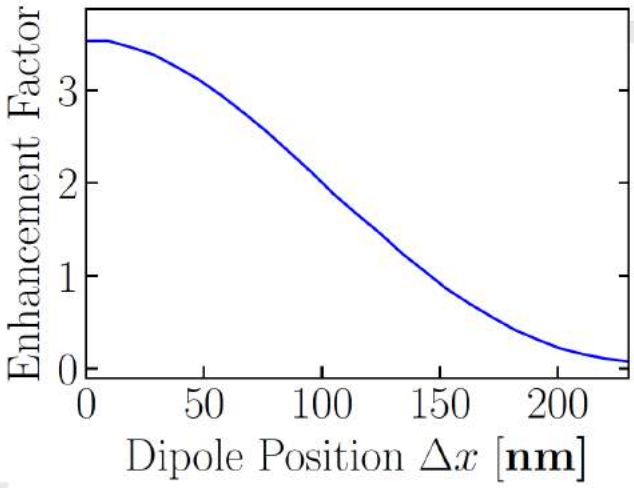

Figure 7: *The effect of moving a dipole source away from the centre of a plasmonic device. The example given is specifically for an optimised ring device however similar relationships can be shown for other plasmonic devices.*

Provided that the nanodiamond clusters are small enough such that the plasmonic device does not actively block any of the nondiamond cluster the cluster will still demonstrate an enhancement and as such the ability for a single diamond nitrogen valency centre to be enhanced through the use of a plasmonic device. As nanodiamonds cannot be used in water the nanodiamond slurry will have to be deposited onto a surface.

4.2 Imaging emission of a surface on the nanoscale.

In order to determine the size and location of nanodiamond on a surface an experiment to be able to image a sample with a resolution of the order of nanometres. The experiment also needs to be capable of illuminating the imaged area with light such that the nanodiamonds can be excited and requires a number of filters such that the photoluminescence of the nanodiamonds can be separated out and imaged from the surface of the sample.

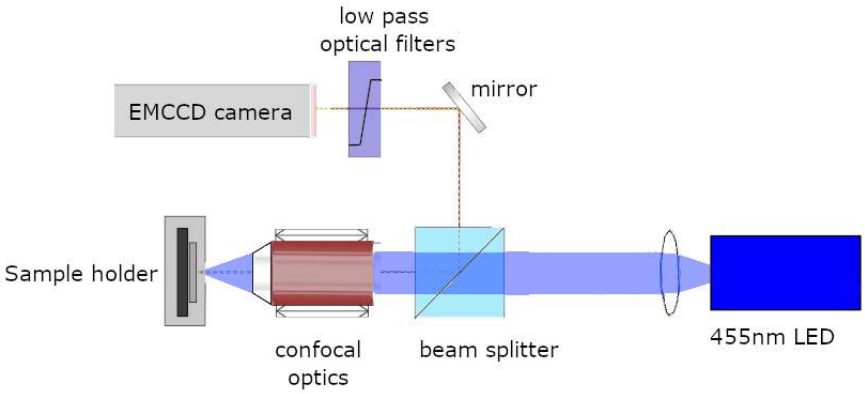

Figure 8: *An experimental set up for imaging the photoluminiscence of a sample with nanometre accuracy. A blue led is focused onto the sample and and the emission collected and directed to a electron multiplying charged coupled device for the purposes of imaging.*

The experimental set up described in figure 8 is capable of focusing light onto a sample and collecting light from the sample through the use of confocal optics and hence is capable of imaging a sample of a micrometre scale. Each individual pixel of this setup represents a square with an area of $7767.718 \pm 0.001 nm^2$ ($88.13nm$ sides of a square). As such a single pixel can in fact support multiple 27nm scale nanodiamonds within it. Thankfully this is not a problem with the expectation that small clusters of nanodiamond will be imaged but would be a further problem if single nanodiamonds are desired as multiple 27nm scale nanodiamonds could fit within a single pixel.

4.3 Deposition recipe determination

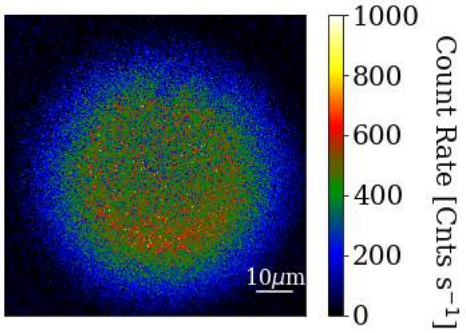

Figure 9: *An image of a clean silicon nitride chip as taken by the experimental set up described in section 4.2.*

Figure 9 shows an image of a clean silicon nitride chip taken with the experimental set

up described in section 4.2. The large circle showing the small section of the imaged chip being illuminated and the variations of colour in this circle are either due to the noise or variations in the surface properties of silicon nitride effecting how the light used to illuminate the sample is reflected.

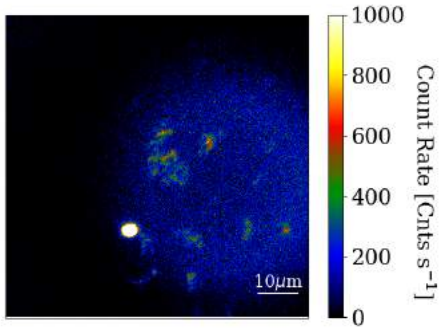

Figure 10: *An image of 0.001 percentage by weight nanodiamond slurry drop cast onto a silicon nitride chip after sonification at 230V, 60 Hz, 350 W (Fisherbrand ultrasonicating water bath, FN11002) for a period of 5 minuites.*

Figure 10 shows the deposition of 27nm nanodiamonds in a solution of water at a density of 0.001wt% which has been aggerated by sonification for a period of 5 minutes. The image clearly shows a single large cluster towards the centre of the image along with a a number of smaller nanodiamond clusters in close proximity to one another.

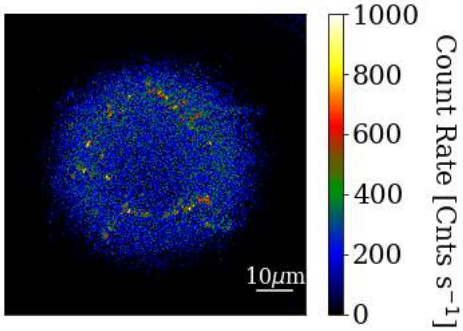

Figure 11: *An image of 0.00005 percentage by weight nanodiamond slurry drop cast onto a silicon nitride chip after sonification at 230V, 60 Hz, 350 W (Fisherbrand ultrasonicating water bath, FN11002) for a period of 30 minuites.*

Figure 11 shows the nanodiamonds, further diluted into a 0.00005wt% that were sonicated for the longer time of 30 minutes. The increased dilution is used in order to make the nanodiamonds more disperse as the plasmonic devices should several micrometres away from one another to prevent them coupling together. (Kino et al.,

2007) The sonification for the extended period is used to reduce the size of the clusters. Ultimately however further sonification will not reduce the size of these clusters further due to the limits as to how effectively sonification can aggregate nanodiamonds. (Ōsawa, 2008)

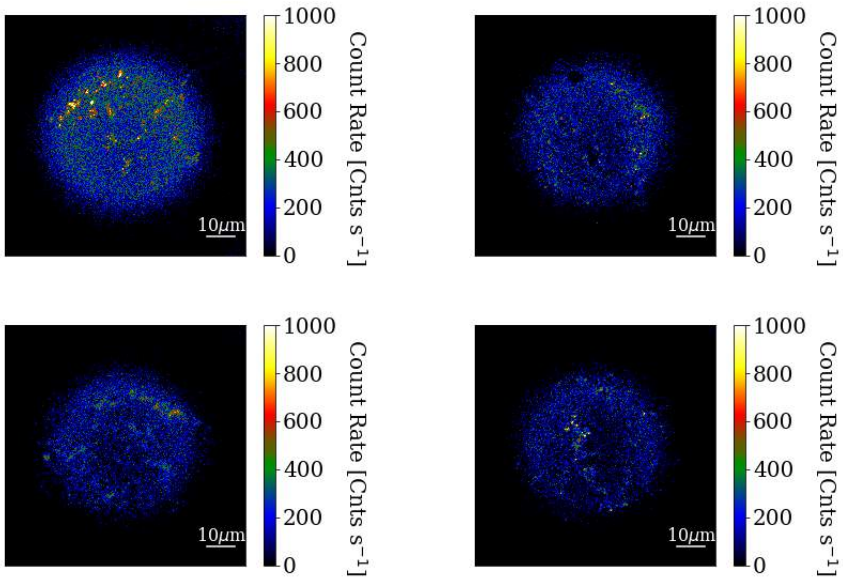

Figure 12: *An image of 0.00005 percentage by weight nanodiamond slurry drop cast onto a silicon nitride chip multiple times after sonification at 230V, 60 Hz, 350 W (Fisherbrand ultrasonicating water bath, FN11002) for a period of 30 minuites. Top left: One application. Top right: Two applications Bottom left: Three applications. Bottom right: Four applications.*

Figure 12 shows what happened when the nanodiamond solution used to obtain the image used in figure 11 is deposited onto the same sample multiple times. From this is it possible to determine how many applications are required in order to obtain enough nanodiamond clusters such that multiple devices can be made but not so many as multiple clusters are effected by the same plasmonic device at once.

5 Fabrication

5.1 Marker Fabrication

With the recipe for minimising the size of nanodiamond clusters while maintaining an optimum dispersion determined it becomes necessary to measure the same nanodiamond cluster consistently. In order to do this nanodiamonds must be prevented from moving and some sort of markers applied to the surface of the sample such that the same place on the sample can be consistently found.

First to prevent the issue with nanodiamonds not being fixed in place a layer of Indium Tin Oxide is deposited onto the silicon nitride chip through sputter deposition. While the intention was to have this layer 15nm thick in practice due to limitations in the spluttering process the layer formed is 15.12nm thick. This has the effect of changing the results expected between the simulations made in section 3 and the actual enhancements measured however the change of 0.12nm does in this region does not make a large change in enhancement measured as is demonstrated in figure 13.

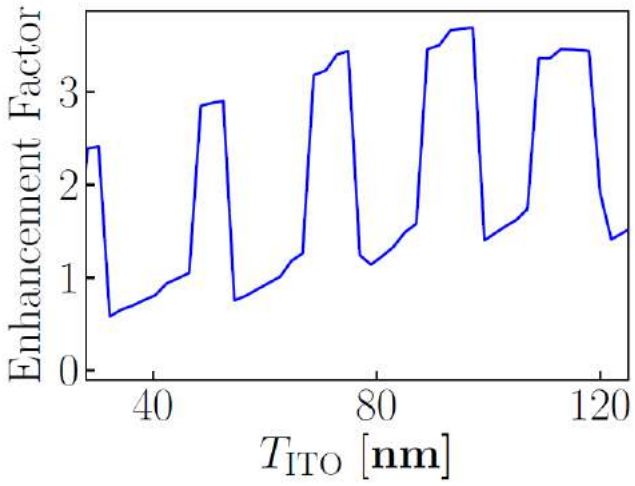

Figure 13: *The effect of Indium Tin Oxide Thickness on the enhancement due to a plasmonic device. The example given is specifically for an optimised ring device however similar relationships can be shown for other plasmonic devices.*

With this layer in place the nanodiamonds are capped and as such cannot be moved from the silicon nitrate surface. This has the additional effect of increasing the critical angle from which emissions can enter free space when compared to bulk diamond due to the effects described in section 2.2.

Markers applied to the surface of the chip need to be of a known size of the order of nanometres such that they are detectable by the imaging process described in section 4.2 but will not dominate the image. In order to obtain such detailed markers Electron Beam Lithography is used.

The sample is covered in two layers of photo-resist. First methyl methacrylate, a low-resolution photo resist such that after the markers are made they remain attached to the sample during the manufacturing process. Then a layer of polymethyl methacrylate, a higher resolution photo-resist, is placed on top such that the dimensionality of the markers corresponds to that which is expected. Electron Beam Lithography is the method of exposing parts of these photo-resist layers through the use of an Electron Beam such that parts of the photo-resist can be removed and a negative of the desired markers made. The sample then has 7nm of chromium deposited onto it through the use of vapor evaporation. This layer is used as an adhesive between the indium tin oxide layer and the layer of gold that follows it. The gold also being deposited via vapor evaporation. When the photo-resist layers are removed all that is left behind on the sample are markers of the desired shapes and dimensions. Gold itself used due to it's resistance to tarnishing as reflections are important for the purposes of imaging the markers through the method described in section 4.2.

Figure 14 shows these markers, a number of labelled grids made across the surface of the sample. Taking both a Scanning Electron Microscope Image and an image using the optical process described in section 4.2. The Scanning Electron Microscope not only allows the sample to be imaged at a wider view possible with the optical process but allows the dimensions of the grid to be checked with a greater degree of accuracy than the same imaging process.

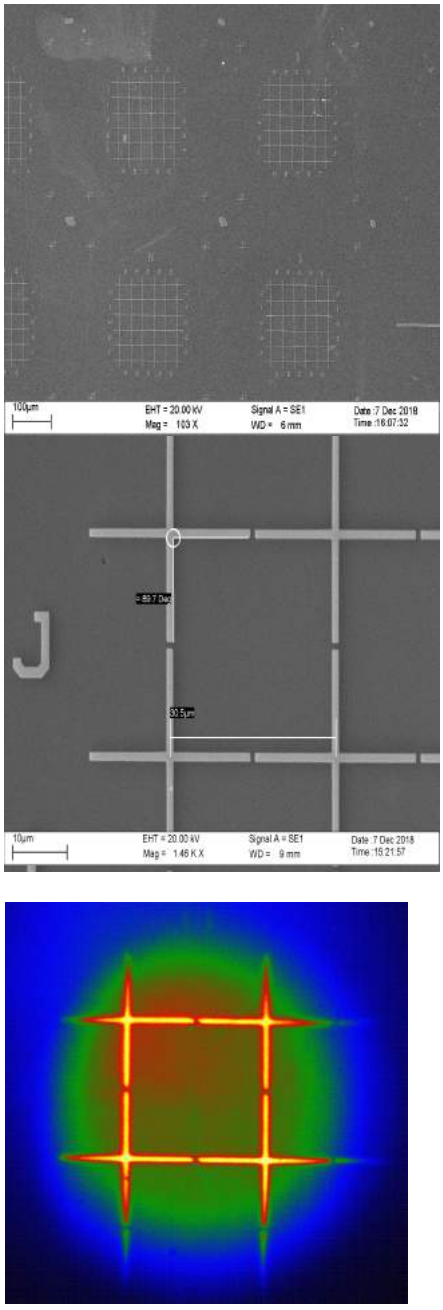

Figure 14: *Marker grids used to consistently the same place of the sample chip. Top: A zoomed out image showing multiple grids. Middle: A image showing the size of the individual grid squares. Bottom: How grid squares appear when optically imaged by the process explained in section 4.2.*

5.2 Fabrication of plasmonic devices

While from simulations many nanophotonic devices demonstrate an enhancement for diamond nitrogen valency centres there is also the limitation in the ability to create

such devices. The sharp points that make up the triangles of the maltese cross are a potential issue. As is the proximity between rings for the concentric ring patterns. As such devices need to not only need to be accurate but also consistently reproducible. As such it is better to test if such devices can be manufactured before attempting to apply them onto the sample.

The method for manufacturing such plasmonic devices is not dissimilar to the method used to create the grids used to mark the sample as described in section 5.1. There being a small number of important differences.

The first major difference is that the methyl methacrylate layer is not used. Due to the size proximity between devices only high-resolution resist can be used. Methyl methacrylate having the potential to undercut the poly-methyl methacrylate layer and the destroy the structure of the devices during the electron beam write process. This means that the lift off process becomes more difficult, potentially resulting in the removal of devices entirely.

The second difference is that due to the removal of this methyl methacrylate layer the dosage required to obtain the correct dimensions of the devices is no longer known. As such the during the testing process many dosage factors need to be tested.

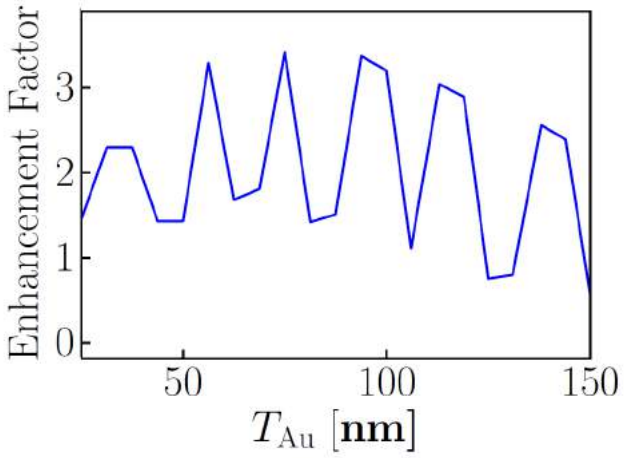

Figure 15: *The effect of gold thickness on the enhancement due to a plasmonic device. The example given is specifically for an optimised ring device however similar relationships can be shown for other plasmonic devices.*

The third difference is that the thickness of the gold layer is specified by the simulations (instead of only need to exist for the purposes of reflection as the grid). While the relationship between gold thickness is a series of peaks as demonstrated by figure 15 the locations of these peaks is different for each plasmonic device and if being manufactured simultaneously these devices cannot be given different gold thicknesses a thickness has to be determined which gives optimum enhancements for each plasmonic device.

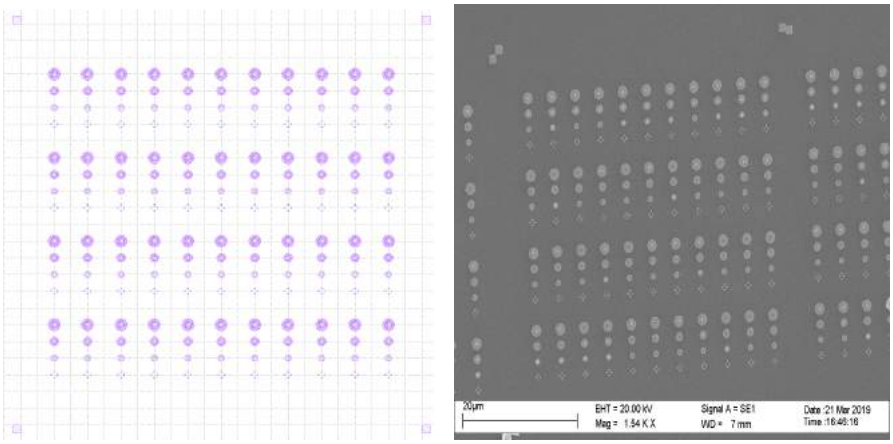

Figure 16: *Right: Device testing pattern. Left: result of manufacturing process taken at a dosage factor of 1.6.*

Figure 16 shows the test write design and the a result from the test write at a particular dosage factor. This demonstrates that the maltese cross, while consistently producible also shows the devices created are not ideal. The individual triangles what form the device having rounded corners. This is expected. Electron beam lithography is never going to produce perfectly sharp corners such as those used in the simulations due to the limitations of the beam shape and the limitations of how polymethyl methacrylate reacts to being exposed to the electron beam itself. It also demonstrates that rings, while producible have the potential to fail, either by not forming complete rings or due to forming complete disks instead of rings. 29 out of a produced 44 being of satsafactory quality. It is worth note that while disks can result in an enhancement (Hao and Schatz, 2004) this enhancement is not as strong as that gained from rings and the optimised dimensions of the disks that produce optimum enhancement are much smaller in scale than those of the rings.

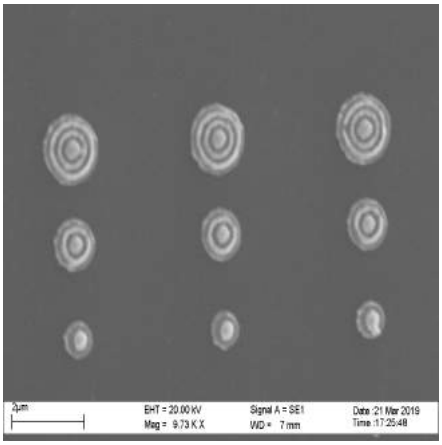

Figure 17: *The structure of concentric ring devices taken at a dosage factor of 0.8 but otherwise made identically to the devices used to manufacture the devices in image 16.*

Figure 17 shows that at lower dosage factors than the optimum dosage factor for the maltese cross and single rings can potentially form concentric rings however there is still metal present between each of the desired rings, implying that producing rings is beyond the scope achievable by the manufacturing methods available. As such despite exhibiting a larger theoretical enhancement cannot be practically tested.

6 Analysis method

6.1 Spectral analysis

With the nanodiamonds deposited and consistently locatable it becomes necessary to determine the emission of the nanodiamond clusters such that the effect of depositing the plasmonic device over it can be determined.

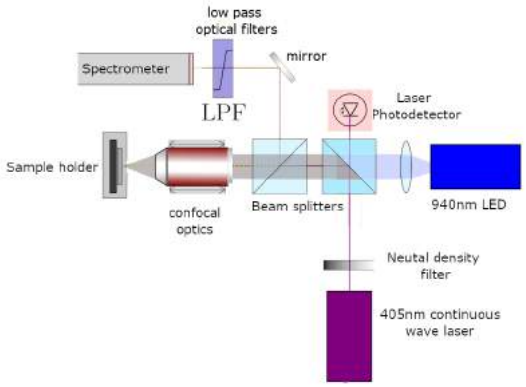

Figure 18: *An experimental set up for measuring the spectrum of a nanodiamond cluster. The infra-red LED is used to measure image grid reflections as so to determine the location of on the grid before peforming the spectral analysis. Note that this experimental set up has minor modifications when compared to the experimental set up used in figure 8.*

Figure 18 shows a modified version of the experimental set up utilised in figure 8. In the place of using a blue LED in order to image a wide area of the sample a blue laser is capable of delivering much higher powers to an area of $573000 \pm 6000nm^2$. Using this laser to excite a small cluster of nanodiamonds photoluminescence from the nanodiamond cluster is directed into a spectrometer instead of an EMCCD camera which can be used to perform spectral analysis of the cluster.

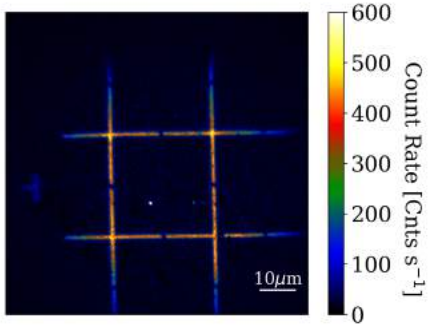

Figure 19: *An image obtained by the equipment in the configeration demonstrated in figure 8 showing a grid and a nanodiamond cluster within the bounds of the grid. This particular nanodiamond cluster is was used for the purposes of aligning the equipment between days and as such did not have a plasmonic device manufactured over it.*

Figure 19 shows an image initially taken with the equipment used in figure 8 showing

both the grid and a nanodiamond cluster contained within the grid. Focusing the blue laser onto this nanodiamond cluster and performing spectral analysis from the emission results in the spectral graph shown in figure 20.

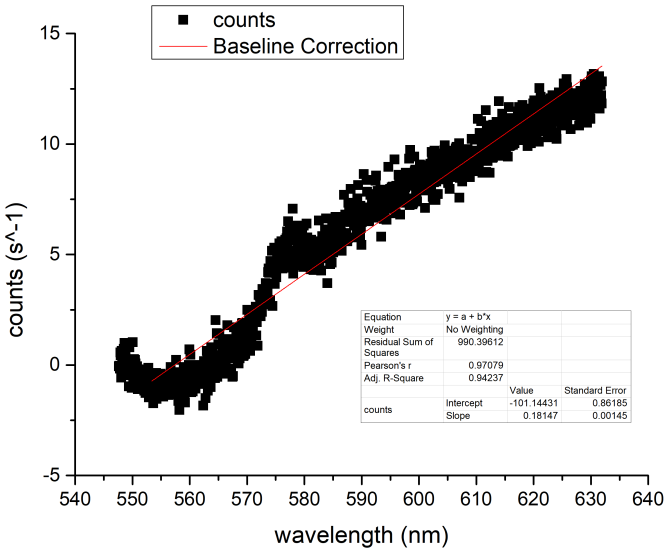

Figure 20: *The raw output of the spectrum taken from the nanodiamond clusted shown in image 19. Note that the full spectrum is not used in the baselign correction due to the action of the optical filters.*

In this state however the spectral information is not usable. As such a baseline correction is made on the spectral data such that the zero phonon line of the diamond nitrogen valency centres can be obtained as shown in figure 21.

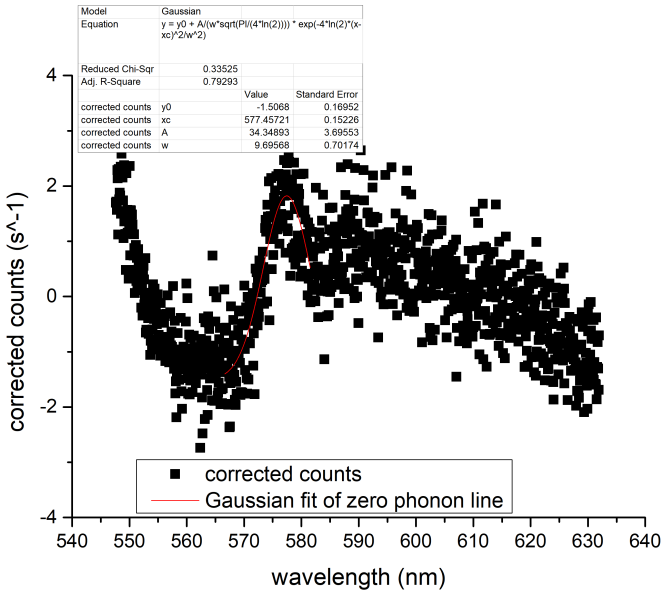

Figure 21: *The same spectrum taken as figure 20 however with a baseline correction.*

From the full width half maximum and the area of this peak fit the height of the peak can be obtained. Note that due to this method, the baseline corrected spectrum does not need to be corrected for non-zero offset. By measuring the emission at varying laser intensities a power series can be formulated such as the one shown in figure 22.

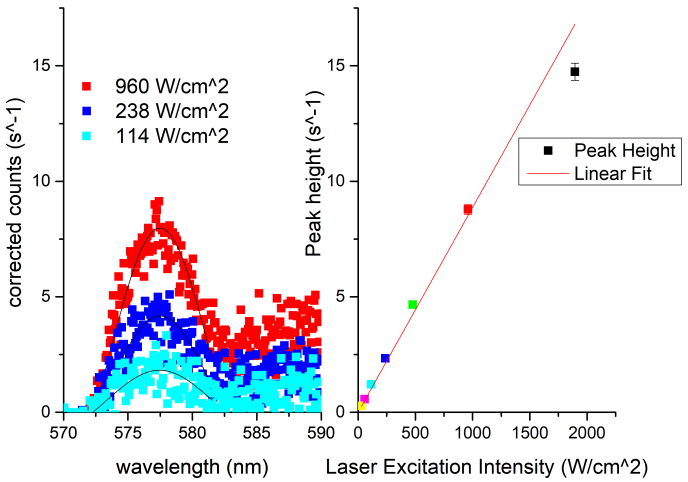

Figure 22: *A graph showing the relationship between the specral data and the resulting power series. Note that the Peak heights may not align perfectly to the corrisponding point on the power series due to zero offset.*

As clusters of nanodiamond are being excited it is unlikely that the ensemble of diamond nitrogen valency centres will reach saturation with powers obtainable by the laser and as such power series relationships for clusters of nanodiamonds will primarily be linear, especially towards the lower end of the scale.

6.2 Manufacturing plasmonic devices for enhancement

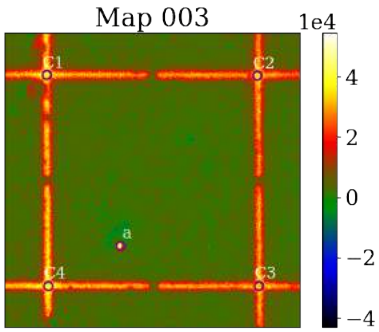

Figure 23: *A nanodiamond cluster in a grid used as an example for the manufacturing method technique.*

Knowing that it is now possible to make the required dimensions of the single ring and maltese cross plasmonic devices it comes to making the plasmonic devices in the correct places. Figure 23 shows a nanodiamond cluster in a grid square. Now knowing both the dimensions of the grid squares and the fact that the grid squares have right angled corners. It is possible to locate the position of the nanodiamond cluster as a fraction of the grid squares. A program takes an image and extracts information as to the horizontal and vertical slices of the program.

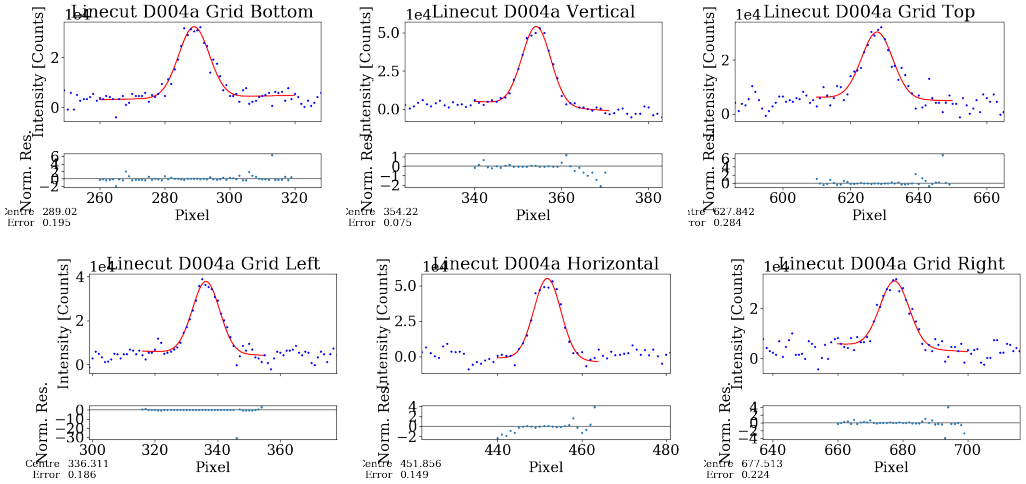

Figure 24: *The output of a program desgined to find the location of nanodiamond clusters. The important data from these graphs is summarised as the value marked Centre in the bottom left of each graph.*

Figure 24 demonstrates the output of this program however the important values are the values labelled centre in the bottom right of each graph. For example the horizontal slice the left side of the square is located at pixel number 336. The cluster cantered on pixel number 452 and the right side of the square is located at 678. From this the cluster can be determined to be $\frac{452-366}{678-366} = 27\%$ of the way from the left side to the right side (with the errors given). Repeating this process, horizontally and vertically for each location where a plasmonic device is required leaves a list of positions where devices can be written.

Now knowing that the devices can be written and knowing where the devices need to be written too with respect to the grid it is now possible to write the devices onto the sample chip itself. This write process is practically identical to the process described in section 5.2 however now the dosage required is known (such that an array of devices is no longer needed) and instead of manufacturing on any arbitrary location on the chip has to first be aligned to the grid before the device is written.

6.3 Enhancement determination method

Each cluster of nanodiamonds with a plasmonic device written on it had its power series taken before the plasmonic device was written on it. Through the same method described in section 6.1 the power series can be taken again. Quantifying enhancement however requires an assumption. As the nanodiamond clusters are not being saturated by the laser it is not possible to directly compare these saturation points in order to determine the enhancement. Instead an assumption that in both cases as power goes to zero, the height of the zero-phonon line also goes to 0. Under these assumptions it becomes possible to compare the values of the linear fits.

7 Enhancement due to manufactured devices

7.1 Square 1

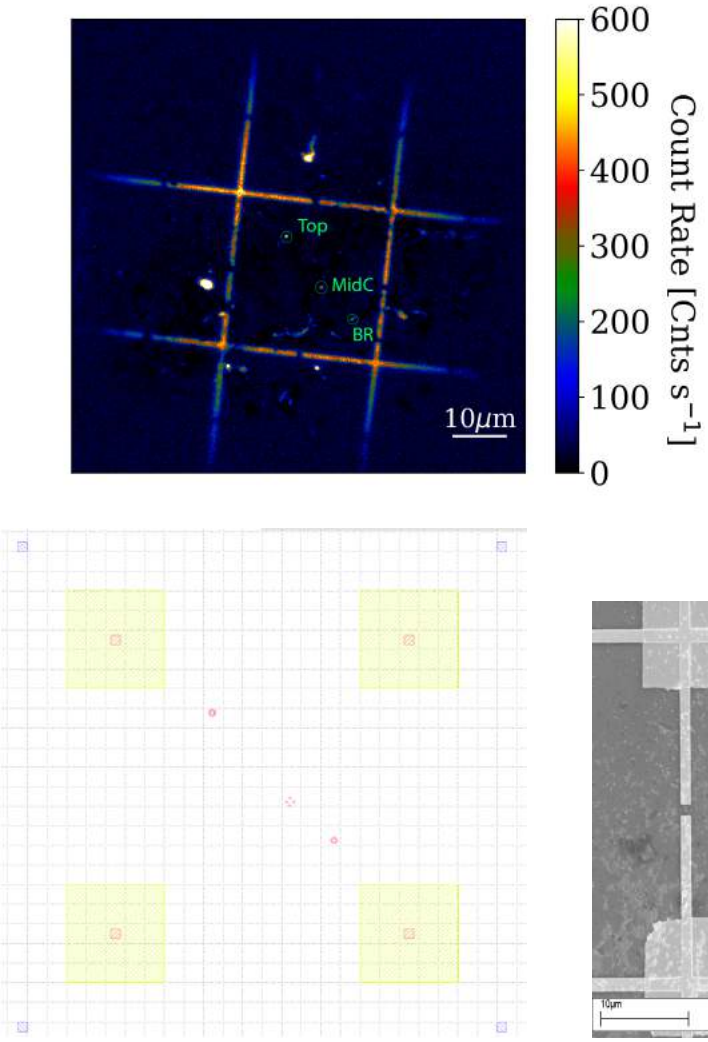

Figure 25: *Top: The photoluminescence image demonstrating three nanodiamond clusters in the same grid square. Bottom left: The desgin manufactured over this grid square. Bottom right: A scanning electron microscope image of this square after the manufacturing process has taken place.*

Grid square shown in figure 25 shows a grid square with three nanodiamond clusters. Labelled Top, MidC and BR. The intended shapes designed written onto this grid and the outcome of the manufacture process.

7.2 Top Result

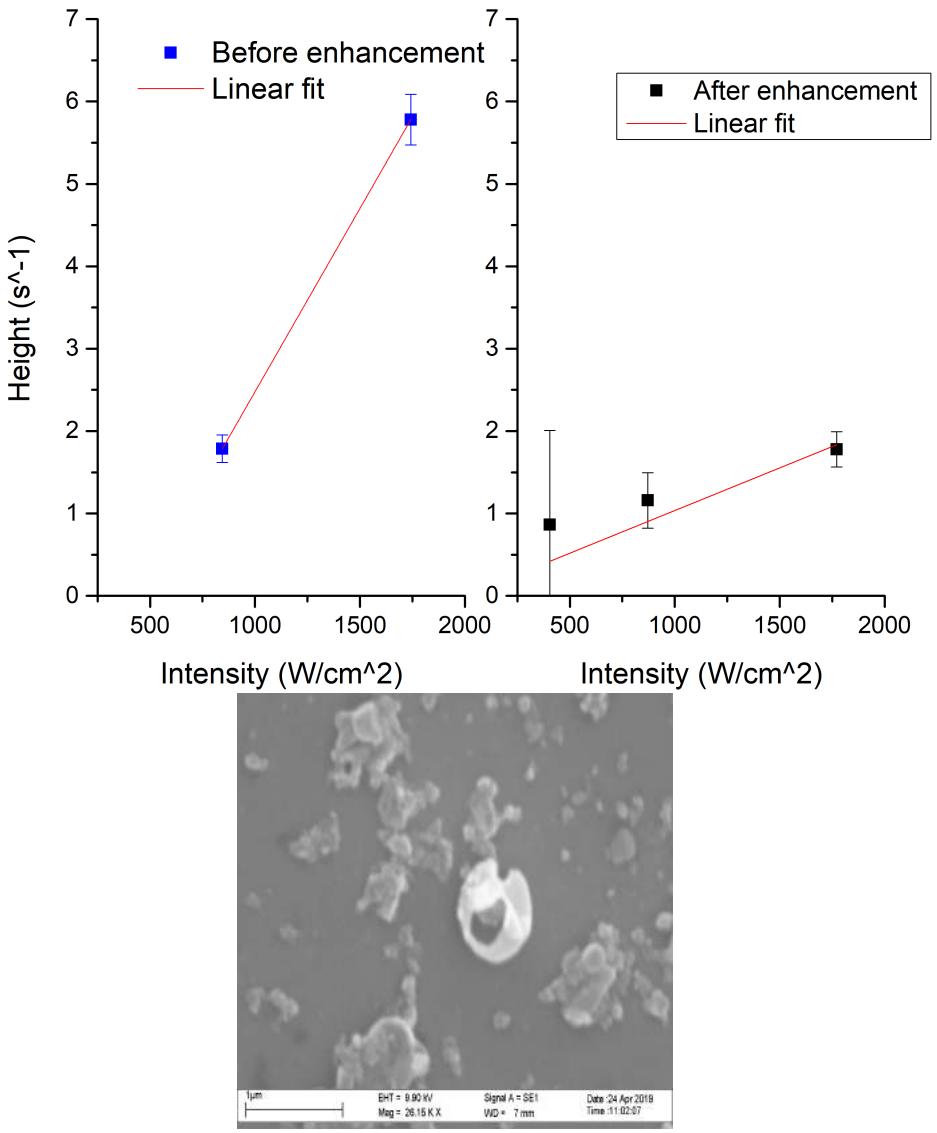

Figure 26: *Top left: A Power series of the nanodiamond cluster taken before plasmonic device deposition. Top right: A Power series of the nanodiamond cluster taken after plasmonic device deposition. Bottom: A zoomed in Scanning Electron Microscope of the plasmonic device formed intended to be a ring.*

Figure 26 shows that while intended to be a ring the device in this location was not manufactured correctly and that the presence of this incorrectly manufactured device resulted in an overall reduction in the detectable emissions from the

associated nanodiamond cluster. Specifically an enhancement factor of 0.26 ± 0.11 is calculated.

7.3 MidC Result

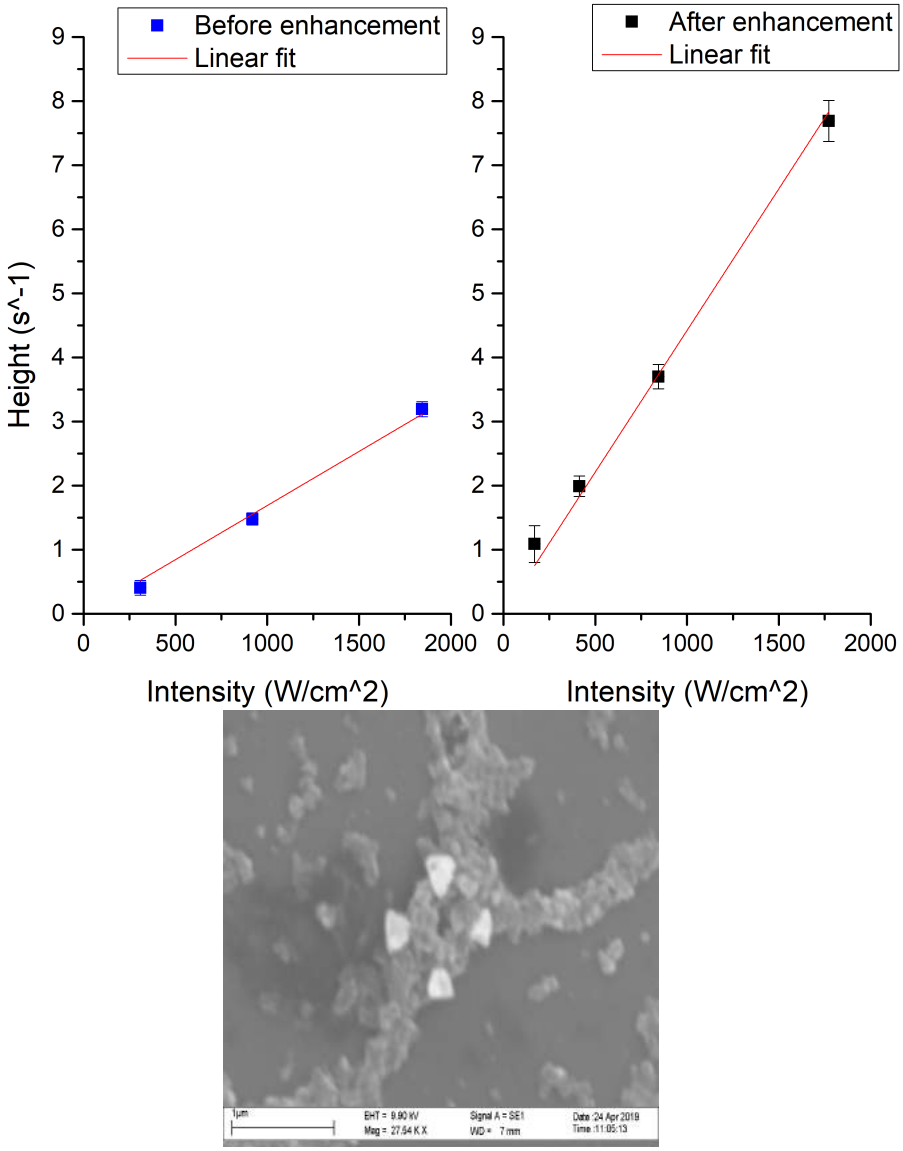

Figure 27: *Top left: A Power series of the nanodiamond cluster taken before plasmonic device deposition. Top right: A Power series of the nanodiamond cluster taken after plasmonic device deposition. Bottom: A zoomed in Scanning Electron Microscope of the plasmonic device formed a maltese cross.*

Figure 27 shows that the Maltese cross formation was successfully manufactured over the nanodiamond cluster and that the presence of the Maltese cross resulted in a quite clear enhancement. However whereas before enhancement took place the errors in peak height are minimal after enhancement takes place errors are noticeable increased. The graphs given only relate power series taken between two days, one before enhancement took place, one after enhancement took place. When multiple datasets are taken both sides of the plasmonic device deposition are taken into consideration these errors increase. As such the enhancement factor is calculated to be a factor of 1.60 ± 1.02. Which while suggesting an enhancement is a significant margin of error, implying that enhancement could not only be much better, but could also be demonstrating a reduction in photon emission.

7.4 BR Result

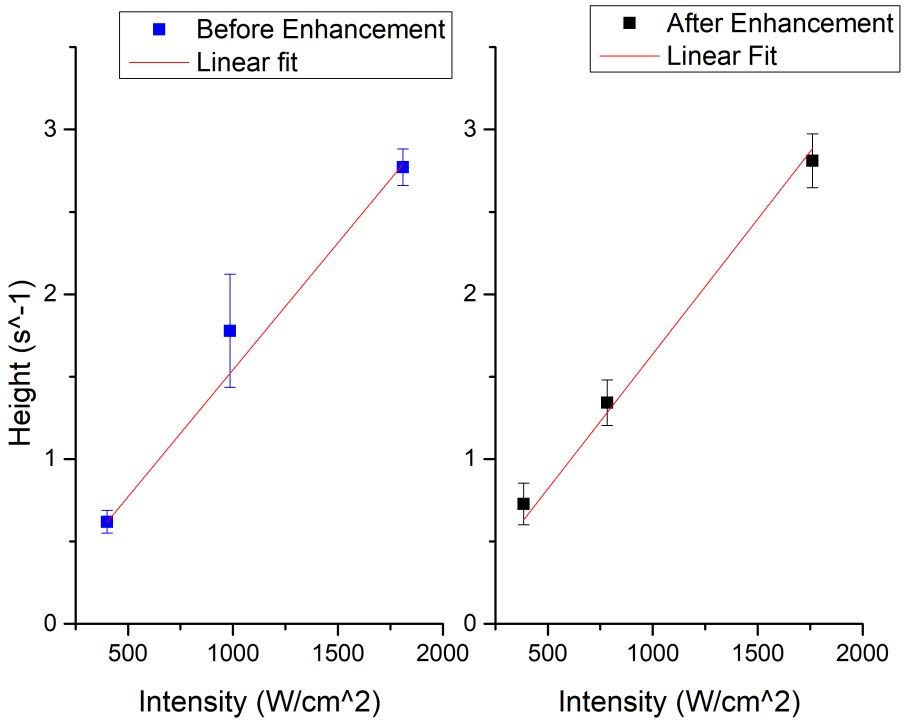

Figure 28: *Left: A Power series of the nanodiamond cluster taken before plasmonic device deposition process was meant to taken place. Top right: A Power series of the nanodiamond cluster taken after plasmonic device deposition process was meant to taken place.*

While intended to be a ring Scanning electron microscope imaging reveals that, presumably during the lift off process, the plasmonic device was removed from the sample. As such the power series graphs being approximately equivalent to one another

is to be expected. As effectively no plasmonic device was made in this location. When properly calculated the enhancement factor is found to be 0.83 ± 0.23. Which while implying a minor reduction to the photon emission is within error of there being no change between both before and after the plasmonic device manufacturing process took place.

7.5 Grid square 2

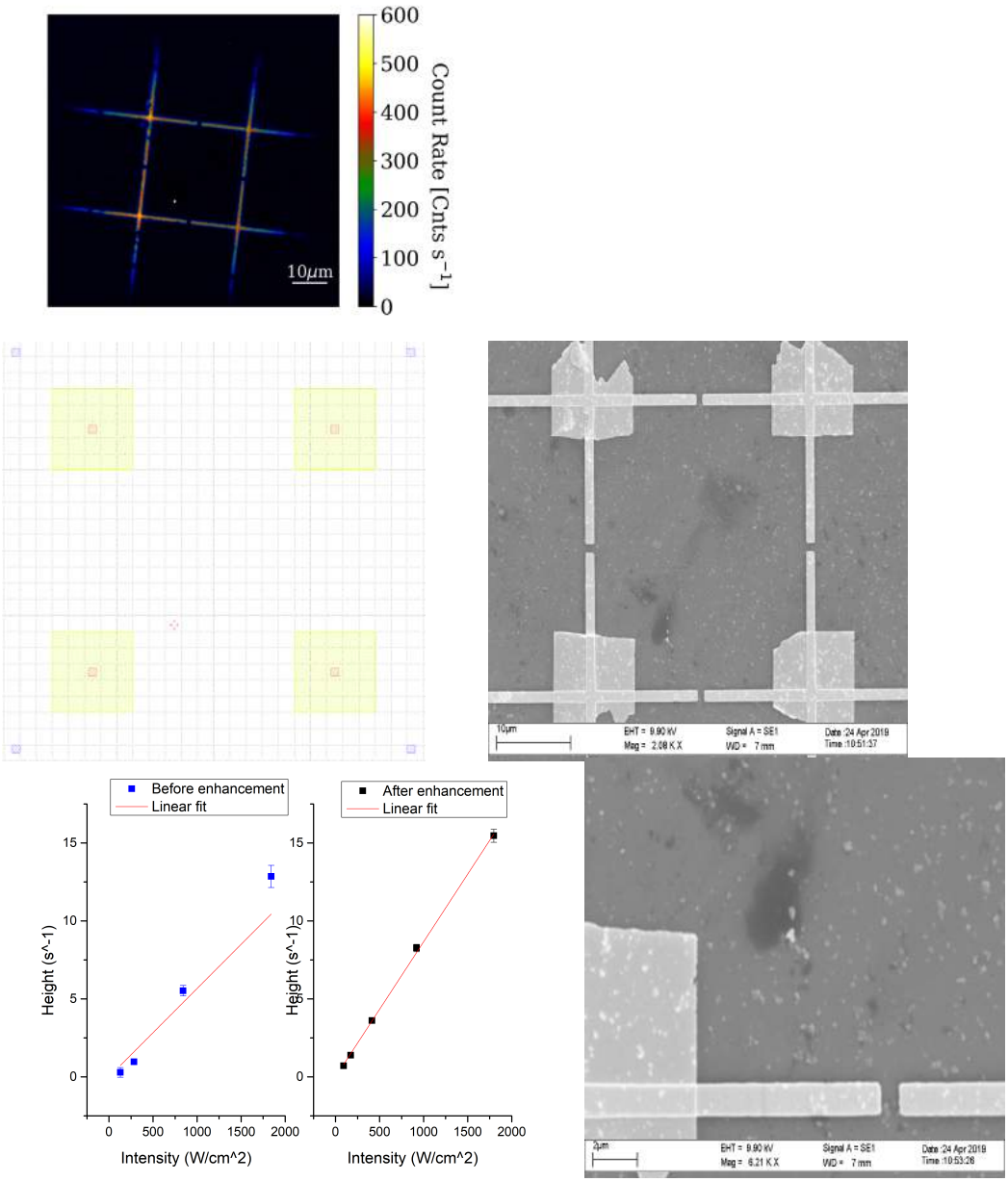

Figure 29: *Top: The photoluminescence image demonstrating a nanodiamond cluster in the a grid square. Middle left: The desgin manufactured over this grid square. Middle right: A scanning electron microscope image of this square after the manufacturing process has taken place. Bottom left: : A Power series of the nanodiamond cluster taken before plasmonic device deposition. Bottom centre: A Power series of the nanodiamond cluster taken after plasmonic device deposition. Bottom right: A zoomed in Scanning Electron Microscope of the plasmonic device formed. A partially formed maltese cross.*

This second square (figure 29) with a second shows only a single nanodiamond cluster which was intended to have a maltese cross made on top of it. The manufacture of this cross, while flawed, was not a complete failure. Only two, opposite, triangles of the maltese cross device came out on the sample. The other two presumably lost during the lift off process. However this flawed maltese cross device is, a bowtie device, which is known to be capable of enhancement. Furthermore the power series does imply an enhancement occurred. When calculated this enhancement factor is 1.55 ± 0.18. Which means that even in the worse possible case of errors this plasmonic device still demonstrated an enhancement in the diamond nitrogen valency centre emission.

7.6 Grid square 3

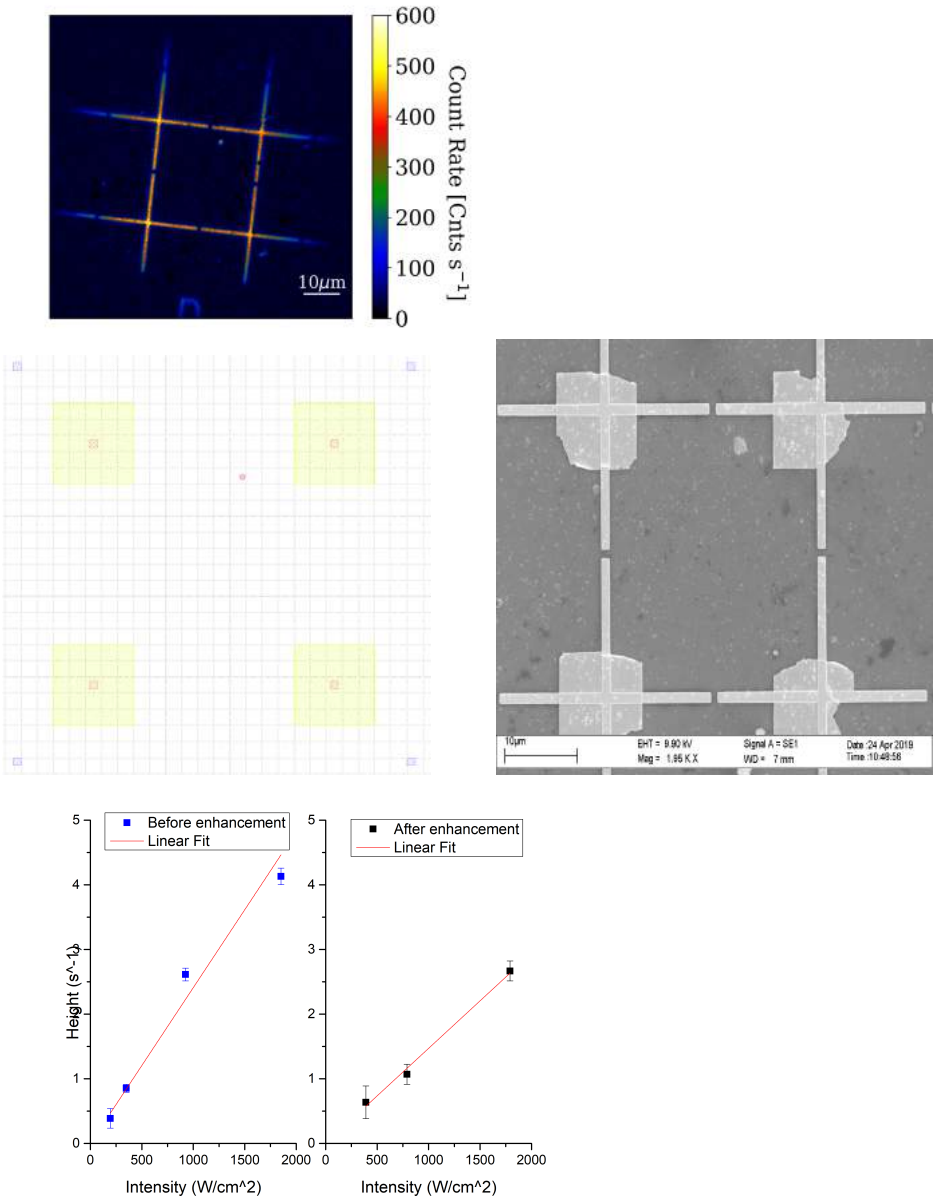

Figure 30: *Top: The photoluminescence image demonstrating a nanodiamond cluster in a grid square. Middle left: The desgin manufactured over this grid square. Middle right: A scanning electron microscope image of this square after the manufacturing process has taken place. Bottom left: : A Power series of the nanodiamond cluster taken before plasmonic device deposition. Bottom right: A Power series of the nanodiamond cluster taken after plasmonic device deposition.*

This third grid square (figure 30) also has a single nanodiamond cluster within it and while intended to be a ring shape either something moved during the electron beam

writing process or the area the ring was intended to go was over exposed as such there is gold present over the nanodiamond cluster however the shape of this deposited shape is not recognisable as any kind of ring. This misshapen gold layer results in the emission from the nanodiamond cluster being reduced. Specifically an enhancement of 0.65 ± 0.04 is found.

8 Conclusions

The average enhancement in emission due to the Maltese cross formation is 1.57 ± 0.51 which is within error of the enhancement of 1.7 determined from computerised simulations of the Maltese cross formation and even in the worse case errors do not allow enhancement to fall below 1 (which would represent a reduction in emission). This demonstrated that overall, the addition of the maltese cross architecture results in an enhancement of the emission from diamond nitrogen valency centres.

Ring shaped architectures on the other hand resulted in an average enhancement of 0.52 ± 0.28. Effectively a reduction in emission. However scanning electron microscope images of these devices also informs that these ring shaped architecture are much more prone to failure than maltese cross architectures. Not does the surface of an optimised rings cover 2.5 times the area of the optimised maltese cross ($316672nm^2$ VS $126284nm^2$) but metal is closer to the centre of the optimised device for ring like structures over maltese cross structures ($190nm$ VS $241nm$). As such not only do ring shaped plasmonic devices require higher manufacturing tolerances than maltese crosses but if the manufacture of the device fails, like the majority of disk shaped devices had, the result is worse for the failure of ring shaped architectures. From this it is possible to conclude that plasmonic devices can be used to increase the emission of diamond nitrogen valency centre emission. It is however important to keep in mind the limitations of the manufacturing techniques as faults in manufacture result in a detrimental effect. As such there is plenty of room for improvement. Many plasmonic devices exhibiting an enhancement greater than that offered from the Maltese cross in theoretical simulations being beyond the limits of manufacture. There is also potential for further improvement through the means of repeating results with single nanodiamonds. While from nanodiamond clusters enhancement can be confirmed to occur the use of single nanodiamonds would increase the accuracy of such results. However where as the ability to manufacture other plasmonic devices is a limitation of solely the manufacturing process the ability to isolate, deposit, image and spectrally analyse single nanodiamonds offers several potential issues. Especially considering the ability to resolve such single nanodiamonds.

9 Appendix

9.1 Calculating the scale of pixel and laser spot.

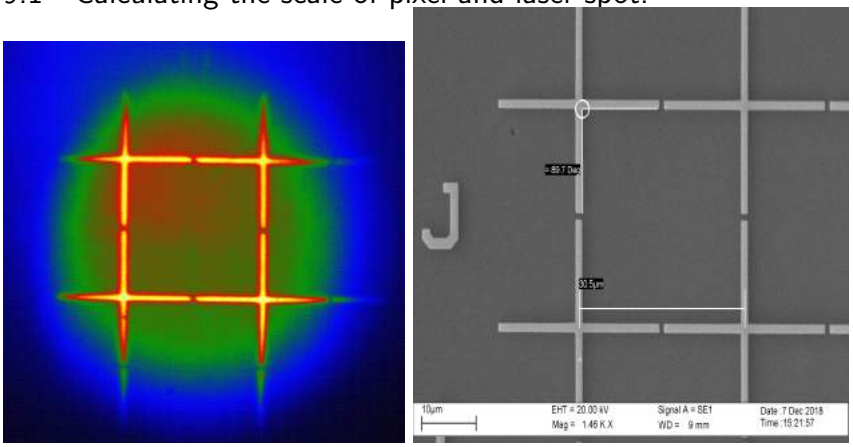

Figure 31: *Left: An image of a grid square taken by the EMCCD camera as described in section 4.2. Right: A Scanning electron microscope image of this same grid square with the dimensionality of the grid marked*

Before grid of known dimensions is made the dimensionality of the camera pixels and laser spot is not known. After the grid is deposited however the EMCCD camera image can be used to determine the size of the camera image. Taking a horizontal slice of the image allows the relationship between pixel size to dimensional size.

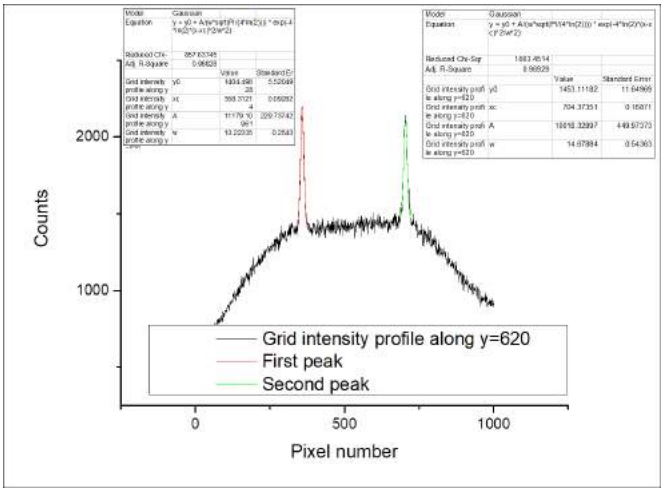

Figure 32: *The count rate located of each pixel located taken as a horozontal slice. The two peaks representing the left and right sides of the grid square.*

With the peaks located at 358.31 ± 0.09 and 704.37 ± 0.17 and as pixels are logically a discrete measure of distance and hence the size of an individual pixel's span can be

found to be 88.13nm and hence the area of an individual pixel found to be $7767.718 \pm 0.001nm^2$.

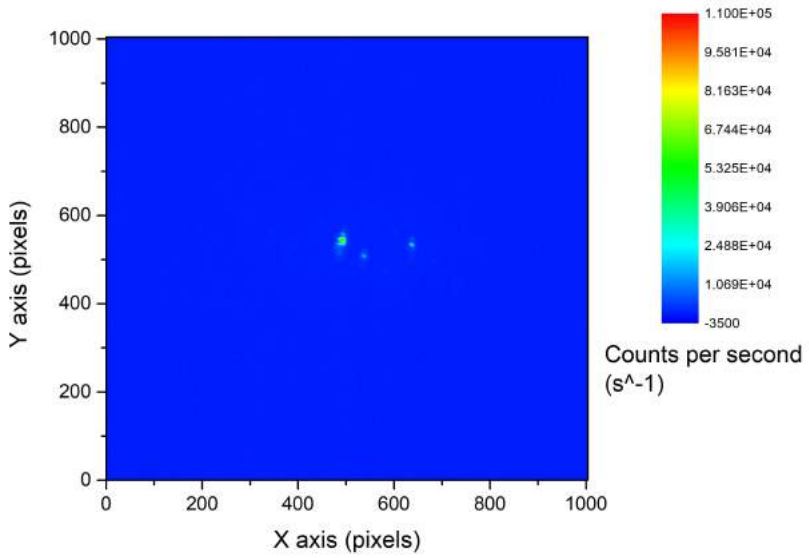

Figure 33: *An image of a the laserspot focused on the surface of a blank sample.*

Similarly the size of the laser can be determined by imaging the laser spot incident on the sample. So taking horizontal and vertical spans of the laser spot and can determine the size in pixels of the laser which can now be related to the actual size of the laser spot.

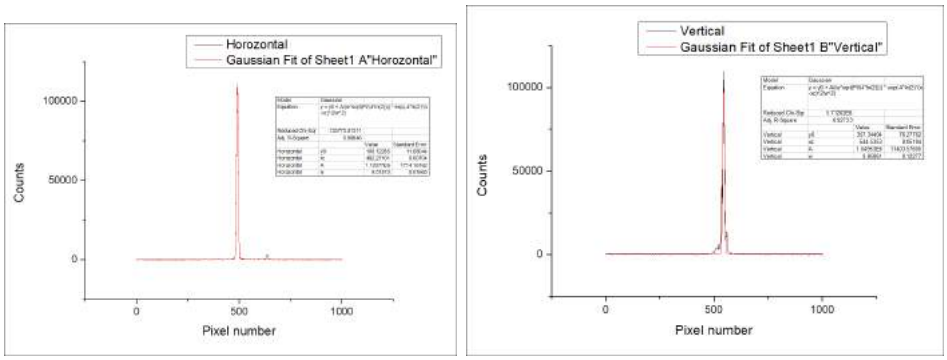

Figure 34: *Left: The count rate located of each pixel located taken as a horozontal slice. The large peak showing the laserspot. Right: The count rate located of each pixel located taken as a Vertical slice. The large peak showing the laserspot.*

$$Horizontal\_width : 9.51 \pm 0.02 pixels$$

$$Vertical\_width : 9.85 \pm 0.12 pixels$$

Which through simple maths and assuming a oval shaped beam becomes

$$Laser\_spot\_area : 573000 \pm 6000 nm^2$$

9.2

References

[1] Aharonovich, I., Greentree, A. and Prawer, S. (2011). Diamond photonics. *Nature Photonics*, 5(7), pp.397-405.

[2] Alkahtani, M., Alghannam, F., Jiang, L., Almethen, A., Rampersaud, A., Brick, R., Gomes, C., Scully, M. and Hemmer, P. (2018). Fluorescent nanodiamonds: past, present, and future. *Nanophotonics*, 7(8), pp.1423-1453.

[3] Grober, R., Schoelkopf, R. and Prober, D. (1997). Optical antenna: Towards a unity efficiency near-field optical probe. *Applied Physics Letters*, 70(11), pp.1354-1356.

[4] Hao, E. and Schatz, G. (2004). Electromagnetic fields around silver nanoparticles and dimers. *The Journal of Chemical Physics*, 120(1), pp.357-366.

[5] Kino, G., Sundaramurthy, A., Schuck, P., Fromm, D. and Moerner, W. (2007). *Optical Field Enhancement with Plasmon Resonant Bowtie Antennas*. Dordrecht: Springer, p.Ch. 9.

[6] König, T., Ledin, P., Kerszulis, J., Mahmoud, M., El-Sayed, M., Reynolds, J. and Tsukruk, V. (2014). Electrically Tunable Plasmonic Behavior of Nanocube–Polymer Nanomaterials Induced by a Redox-Active Electrochromic Polymer. *ACS Nano*, 8(6), pp.6182-6192.

[7] Kuppam, S. (2018). Modelling of Quantum Key Distribution Protocols in Communicating Quantum Processes Language with Verification and Analysis in PRISM. *Proceedings of 8th International Conference on Simulation and Modeling Methodologies, Technologies and Applications.*

[8] Luke, K., Okawachi, Y., Lamont, M., Gaeta, A. and Lipson, M. (2015). Broadband mid-infrared frequency comb generation in a Si_3N_4 microresonator. *Optics Letters*, 40(21), p.4823.

[9] Ōsawa, E. (2008). Monodisperse single nanodiamond particulates. *Pure and Applied Chemistry*, 80(7), pp.1365-1379.

[10] Palik, E. (1995). *Handbook of optical constants of solids*. San Diego: Academic Press Inc.

[11] Phillip, H. and Taft, E. (1964). Kramers-Kronig Analysis of Reflectance Data for Diamond. *Physical Review*, 136(5A), pp.A1445-A1448.

[12] Reithmaier, J., Sek, G., Löffler, A., Hofmann, C., Kuhn, S., Reitzenstein, S., Keldysh, L., Kulakovskii, V., Reinecke, T. and Forchel, A. (2004). Strong coupling in a single quantum dot–semiconductor microcavity system. *Nature*, 432(7014), pp.197-200.

[13] Santori, C., Fattal, D. and Yamamoto, Y. (2010). *Single-photon devices and applications*. Weinheim: Wiley-VCH, p.174.

[14] Shrivastava, A. and Verma, A. (2012). A secure approach of eavesdropper detection in quantum key distribution. *Fourth International Conference on Advances in Recent Technologies in Communication and Computing (ARTCom2012).*

[15] Taflove, A. (1995). *Computational electrodynamics: The Finite-Difference Time-Domain Method*. Boston, Mass.: Artech House.

[16] Trojak, O., Park, S., Song, J. and Sapienza, L. (2017). Metallic nanorings for broadband, enhanced extraction of light from solid-state emitters. *Applied Physics Letters*, 111(2), p.021109.